

Supporting Information

Truncated Tetrahedral RNA Nanostructures Exhibit Enhanced Features for Delivery of RNAi Substrates

Paul Zakrevsky, Wojciech K Kasprzak, William F Heinz, Weimin Wu, Htet Khant, Eckart Bindewald, Nomongo Dorjsuren, Eric A Fields, Natalia de Val, Luc Jaeger and Bruce A Shapiro

RNA sequences used in this study

Nanoring dumbbell scaffold monomers (5' to 3'):

Kissing loop sequences underlined

NR-A: GGGAAUCCGUCCACUGGAUUCCCGUCACAGAGCCUGCCUGUGAC

NR-B: GGGAAUCCGCAGGCUGGAUUCCCGUCACAGAGAACGCUGUGAC

NR-C: GGGAAUCCCGGUUCUGGAUUCCCGUCACAGACGUCUCCUGUGAC

NR-D: GGGAAUCCGAGACGUGGAUUCCCGUCACAGUCGUGGUCUGUGAC

NR-E: GGGAAUCCACCACGAGGAUUCCCGUCACAGAACCAUCCUGUGAC

NR-F: GGGAAUCCGAUGGUUGGAUUCCCGUCACAGAGUGGACCUGUGAC

Nanoring dumbbell monomers functionalized with enhanced green fluorescent protein (eGFP)

DsiRNA antisense (5' to 3'):

Kissing loop sequences underlined; eGFP antisense sequence in bold

NR-A.gfp:

GGGAACCGUCCACUGGUUCCCGCUACGAGAGCCUGCCUCGUAGCUU**CGGUGGUGCAGAUGAACUUCAGGGUCA**

NR-B.gfp:

GGGAACCGCAGGCUGGUUCCCGCUACGAGAGAACGCUCUGUAGCUU**CGGUGGUGCAGAUGAACUUCAGGGUCA**

NR-C.gfp:

GGGAACCGCGUUCUGGUUCCCGCUACGAGACGUCUCUCGUAGCUU**CGGUGGUGCAGAUGAACUUCAGGGUCA**

NR-D.gfp:

GGGAACCGAGACGUGGUUCCCGCUACGAGUCGUGGUCUCGUAGCUU**CGGUGGUGCAGAUGAACUUCAGGGUCA**

NR-E.gfp:

GGGAACCGACACGAGGUUCCCGCUACGAGAACCAUCCUCGUAGCUU**CGGUGGUGCAGAUGAACUUCAGGGUCA**

NR-F.gfp:

GGGAACCGAUGGUUGGUUCCCGCUACGAGAGUGGACCUCGUAGCUU**CGGUGGUGCAGAUGAACUUCAGGGUCA**

Nanoring dumbbell monomers functionalized with negative control (nc1) DsiRNA antisense (5' to 3'):

Kissing loop sequences underlined; nc1 antisense sequence in bold

NR-B.nc1:

GGGAACCGCAGGCUGGUUCCCGCUACGAGAGAACGCUCUGUAGCUU**AUACGCGUAUUAUACGCGAUUAACGAC**

NR-D.nc1:

GGGAACCGAGACGUGGUUCCCGCUACGAGUCGUGGUCUCGUAGCUU**AUACGCGUAUUAUACGCGAUUAACGAC**

NR-E.nc1:

GGGAACCGACACGAGGUUCCCGCUACGAGAACCAUCCUCGUAGCUU**AUACGCGUAUUAUACGCGAUUAACGAC**

NR-F.nc1:

GGGAACCGAUGGUUGGUUCCCGCUACGAGAGUGGACCUCGUAGCUU**AUACGCGUAUUAUACGCGAUUAACGAC**

Nanoring dumbbell monomers functionalized with polo like kinase 1 (plk1) DsiRNA antisense (5' to 3'):

Kissing loop sequences underlined; plk1 antisense sequence in bold

NR-A.plk1:

GGGAACCGUCCACUGGUUCCCGCUACGAGAGCCUGCCUCGUAGCUU**UCGUCAUUAAGCAGCUCGUUAAUGGUU**

NR-B.plk1:

GGGAACCGCAGGCUGGUUCCCGCUACGAGAGAAACGCCUCGUAGCUU**UCGUCAUUAAGCAGCUCGUUAAUGGUU**

NR-C.plk1:

GGGAACCGCGUUCUGGUUCCCGCUACGAGACGUCUCCUCGUAGCUU**UCGUCAUUAAGCAGCUCGUUAAUGGUU**

NR-D.plk1:

GGGAACCGAGACUGGUUCCCGCUACGAGUCGUGGUCUCGUAGCUU**UCGUCAUUAAGCAGCUCGUUAAUGGUU**

NR-E.plk1:

GGGAACCGACAGAGGUUCCCGCUACGAGAAACCAUCCUCGUAGCUU**UCGUCAUUAAGCAGCUCGUUAAUGGUU**

NR-F.plk1:

GGGAACCGAUGGUUGGUUCCCGCUACGAGAGUGGACCUCGUAGCUU**UCGUCAUUAAGCAGCUCGUUAAUGGUU**

Nanoring dumbbell monomers functionalized with eGFP scramble1 DsiRNA antisense (5' to 3'):

Kissing loop sequences underlined; scramble1 antisense sequence in bold

NR-B.scrmb1:

GGGAAUCCGCAGGCUGGAUCCCGUCACAGAGAAACGCCUGUGACUU**GAUGCGCGUAGUCCGUAUGGCUAAGAG**

NR-D.scrmb1:

GGGAAUCCGAGACUGGAUCCCGUCACAGUCGUGGUCUGUGACUU**GAUGCGCGUAGUCCGUAUGGCUAAGAG**

NR-F.scrmb1:

GGGAAUCCGAUGGUUGGAUCCCGUCACAGAGUGGACCUGUGACUU**GAUGCGCGUAGUCCGUAUGGCUAAGAG**

Nanoring dumbbell monomers functionalized with eGFP scramble2 DsiRNA antisense (5' to 3'):

Kissing loop sequences underlined; scramble2 antisense sequence in bold

NR-B.scrmb2:

GGGAAUCCGCAGGCUGGAUCCCGUCACAGAGAAACGCCUGUGACUU**GCUUCCGGGUGCAAUGGAAGGUGAUAC**

NR-D.scrmb2:

GGGAAUCCGAGACUGGAUCCCGUCACAGUCGUGGUCUGUGACUU**GCUUCCGGGUGCAAUGGAAGGUGAUAC**

NR-F.scrmb2:

GGGAAUCCGAUGGUUGGAUCCCGUCACAGAGUGGACCUGUGACUU**GCUUCCGGGUGCAAUGGAAGGUGAUAC**

Tetrahedral nanoparticle "cross-over" monomers (5' to 3'):

Kissing loop sequences underlined; junction sequences in italics

TET-A:

GGUGUCCACUACCCUCGACAGAAUCUGACAUCAGCCUGCGAUGUCUAAGACAUGGUCCACUCAUGUCGACAGAUUCU
GCACAGAGCCUGCCUGUGCUAAGAG

TET-C:

GGUGCGUUCUACCCUCGACAGAAUCUGACAUCACGUCUCGAUGUCUAAGACAUGGCGUUCUCAUGUCGACAGAUUCU
GCACAGACGUCUCCUGUGCUAAGAG

TET-E:

GGGACCACGACCCCGUCGACAGAAUCUGACAUCAACCAUCGAUGUCUAAGACAUGACCACGACAUGUCGACAGAUUCU
GCACAGAACCAUCUGUGCUAAGAG

Nanocube scaffold monomers (5' to 3'):

Cb-A: GGCAACUUUGAUCCCUCGGUUUAGCGCCGGCCUUUUCUCCCACACUUUCACG

Cb-B: GGGAAAUUUCGUGGUAGGUUUUGUUGCCCGUGUUUCUACGAUUACUUUGGUC

Cb-C: GGACAUUUUCGAGACAGCAUUUUUCCCGACCUUUGCGGAUUGUAUUUUAGG

Cb-D: GGCUCUUUUGACCUUCUGUCUUUAUGUCCCCUAUUUCUAAUGACUUUUGGCC

Cb-E: GGGAGAUUUAGUCAUUAAGUUUUACAAUCCGCUUUGUAAUCGUAGUUUGUGU

Cb-F: GGGAUUUUACCUACCACGUUUUGCUGUCUCGUUUGCAGAAGGUCUUUCCGA

Nanocube monomers functionalized with enhanced green fluorescent protein (eGFP) DsiRNA antisense (5' to 3'):

eGFP antisense sequence in bold

Cb-A.gfp:

GGCAACUUUGAUCCCUCGGUUUAGCGCCGGCCUUUUCUCCCACACUUUCACGUU**CGGUGGUGCAGAUGAACUUCAGG
GUCA**

Cb-B.gfp:

GGGAAAUUUCGUGGUAGGUUUUGUUGCCCGUGUUUCUACGAUUACUUUGGUCUU**CGGUGGUGCAGAUGAACUUCAGG
GUCA**

Cb-C.gfp:

GGACAUUUUCGAGACAGCAUUUUUCCCGACCUUUGCGGAUUGUAUUUUAGGUU**CGGUGGUGCAGAUGAACUUCAGG
GUCA**

Cb-D.gfp:

GGCGCUUUUGACCUUCUGUCUUUAUGUCCCCUAUUUCUAAUGACUUUUGGCCUU**CGGUGGUGCAGAUGAACUUCAGG
GUCA**

Cb-E.gfp:

GGGAGAUUUAGUCAUUAAGUUUUACAAUCCGCUUUGUAAUCGUAGUUUGUGUUU**CGGUGGUGCAGAUGAACUUCAGG
GUCA**

Cb-F.gfp:

GGGAUUUUACCUACCACGUUUUGCUGUCUCGUUUGCAGAAGGUCUUUCCGAUU**CGGUGGUGCAGAUGAACUUCAGG
GUCA**

Nanocube monomers functionalized with negative control (nc1) DsiRNA antisense (5' to 3'):

nc1 antisense sequence in bold

Cb-E.nc1:

GGGAGAUUUAGUCAUUAAGUUUUACAAUCCGCUUUGUAAUCGUAGUUUGUGUUU**AUACGCGUAUUUAUCGCGAUUAA
CGAC**

Cb-F.nc1:

GGGAUUUUACCUACCACGUUUUGCUGUCUCGUUUGCAGAAGGUCUUUCCGAUU**AUACGCGUAUUUAUCGCGAUUAA
CGAC**

Nanocube monomers functionalized with polo like kinase 1 (plk1) DsiRNA antisense (5' to 3'):

plk1 antisense sequence in bold

Cb-A.plk1:

GGCAACUUUGAUCCCUCGGUUUAGCGCCGGCCUUUCUCCCACACUUUCACGUUU**UCGUCAUUAAGCAGCUCGUUAAU**
GGUU

Cb-B.plk1:

GGGAAUUUCGUGGUAGGUUUUGUUGCCCGUGUUUCUACGAUUACUUUGGUCUU**UCGUCAUUAAGCAGCUCGUUAAU**
GGUU

Cb-C.plk1:

GGACAUUUUCGAGACAGCAUUUUUUCCCGACCUUUGCGGAUUGUAUUUUAGGUUU**UCGUCAUUAAGCAGCUCGUUAAU**
GGUU

Cb-D.plk1:

GGCGUUUUGACCUUCUGCUUUUUGUCCCCUAUUUCUUAUGACUUUUGGCCUU**UCGUCAUUAAGCAGCUCGUUAAU**
GGUU

Cb-E.plk1:

GGGAGAUUUAGUCAUUAAGUUUUACAAUCCGCUUUGUAAUCGUAGUUUGUGUUUU**UCGUCAUUAAGCAGCUCGUUAAU**
GGUU

Cb-F.plk1:

GGGAUCUUUACCUACCACGUUUUGCUGUCUCGUUUGCAGAAGGUCUUUCCGAUU**UCGUCAUUAAGCAGCUCGUUAAU**
GGUU

Corresponding DsiRNA sense and fluorescently labeled strands (5' to 3'):

(p) denotes a 5' monophosphate; dN denotes deoxynucleotide

eGFP DsiRNA sense:

(p) ACCCUGAAGUUCAUCUGCACCACCG

(6-FAM) eGFP DNA sense; DNA sense strand labeled with 6-carboxyfluorescein (6-FAM):

(6-FAM) dAdCdCdCdTdTdAdAdGdTdTdCdAdTdTdTdGdCdAdCdCdAdCdCdG

nc1 DsiRNA sense:

(p) CGUUAAUCGCGUAUAAUACGCGUAU

plk1 DsiRNA sense:

(p) CCAUUAACGAGCUGCUUAAUGACGA

scramble1 DsiRNA sense:

(p) CUUAGCCAUACGGACUACGCGCAUC

scramble2 DsiRNA sense:

(p) AUCACCUUCCAUUGCACCCGGAAGC

Supporting Tables

Table S1: Monomers used to assemble various RNA nanostructures in this study. The copy number per assembled nanoparticle is indicated for each strand.

Nanoring structures

Core Scaffold	6 eGFP DsiRNA	4 eGFP DsiRNA	6 plk1 DsiRNA	(6-FAM) labeled
NR-A (x1)	NR-A.gfp (x1)	NR-A (x1)	NR-A.plk1 (x1)	NR-A.gfp (x1)
NR-B (x1)	NR-B.gfp (x1)	NR-B.gfp (x1)	NR-B.plk1 (x1)	NR-B.nc1 (x1)
NR-C (x1)	NR-C.gfp (x1)	NR-C.gfp (x1)	NR-C.plk1 (x1)	NR-C.gfp (x1)
NR-D (x1)	NR-D.gfp (x1)	NR-D (x1)	NR-D.plk1 (x1)	NR-D.gfp (x1)
NR-E (x1)	NR-E.gfp (x1)	NR-E.gfp (x1)	NR-E.plk1 (x1)	NR-E.nc1(x1)
NR-F (x1)	NR-F.gfp (x1)	NR-F.gfp (x1)	NR-F.plk1 (x1)	NR-F.gfp (x1)
	eGFP sense (x6)	eGFP sense (x4)	plk1 sense (x6)	nc1 sense (x2)
				(6-FAM) eGFP DNA sense (x4)

Nanocube structures

Core Scaffold	6 eGFP DsiRNA	4 eGFP DsiRNA	6 plk1 DsiRNA	(6-FAM) labeled
Cb-A (x1)	Cb-A.gfp (x1)	Cb-A.gfp (x1)	Cb-A.plk1 (x1)	Cb-A.gfp (x1)
Cb-B (x1)	Cb-B.gfp (x1)	Cb-B.gfp (x1)	Cb-B.plk1 (x1)	Cb-B.gfp (x1)
Cb-C (x1)	Cb-C.gfp (x1)	Cb-C.gfp (x1)	Cb-C.plk1 (x1)	Cb-C.gfp (x1)
Cb-D (x1)	Cb-D.gfp (x1)	Cb-D.gfp (x1)	Cb-D.plk1 (x1)	Cb-D.gfp (x1)
Cb-E (x1)	Cb-E.gfp (x1)	Cb-E (x1)	Cb-E.plk1 (x1)	Cb-E.nc1 (x1)
Cb-F (x1)	Cb-F.gfp (x1)	Cb-F (x1)	Cb-F.plk1 (x1)	Cb-F.nc1 (x1)
	eGFP sense (x6)	eGFP sense (x4)	plk1 sense (x6)	nc1 sense (x2)
				(6-FAM) eGFP DNA sense (x4)

Tetrahedral structures

Core Scaffold	12 eGFP DsiRNA	4 eGFP DsiRNA	12 plk1 DsiRNA	(6-FAM) labeled
TET-A (x2)	TET-A (x2)	TET-A (x2)	TET-A (x2)	TET-A (x2)
NR-B (x4)	NR-B.gfp (x4)	NR-B.gfp (x4)	NR-B.plk1 (x4)	NR-B.gfp (x4)
TET-C (x2)	TET-C (x2)	TET-C (x2)	TET-C (x2)	TET-C (x2)
NR-D (x4)	NR-D.gfp (x4)	NR-D (x4)	NR-D.plk1 (x4)	NR-D.nc1 (x4)
TET-E (x2)	TET-E (x2)	TET-E (x2)	TET-E (x2)	TET-E (x2)
NR-F (x4)	NR-F.gfp (x4)	NR-F (x4)	NR-F.plk1 (x4)	NR-F.nc1 (x4)
	eGFP sense (x12)	eGFP sense (x4)	plk1 sense (x12)	nc1 sense (x8)
				(6-FAM) eGFP DNA sense (x4)

Table S2: Size estimates of the tetrahedral scaffold and functionalized tetrahedral nanoparticles based radius of gyration measurements of corresponding three-dimensional models.

Modeled Structure	Condition	Diameter (nm)
Tetrahedral Scaffold	Initial minimized model	20.0
	Last MD frame at 250ns	21.6
	<i>Average of all MD time steps</i>	<i>21.8 ± 0.5</i>
12DsiRNA Functionalized Tetrahedral Nanoparticle	Minimized model	32.8

Supporting Figures

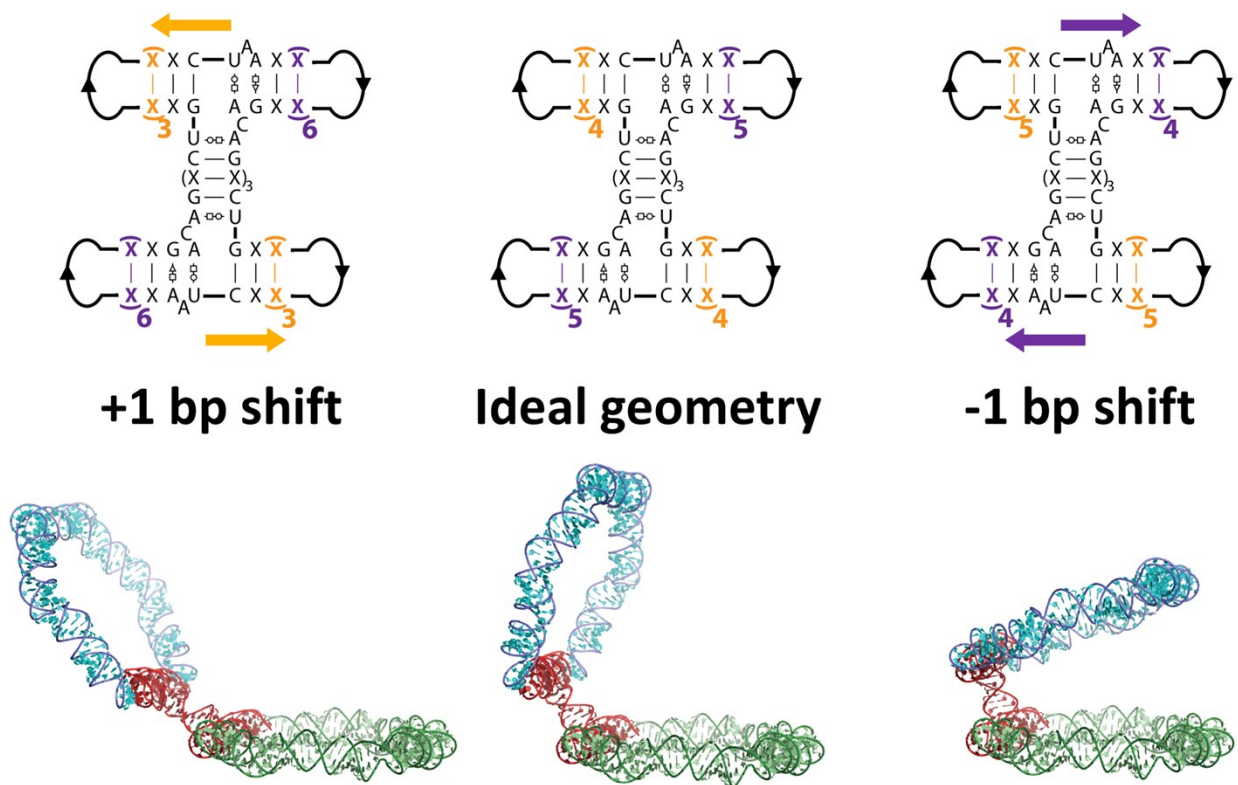


Figure S1. The UAh three-way junction was manually modeled at various positions within adjacent monomers of two nanorings in order to find the best arrangement of neighboring rings that comes closest to producing an ideal tetrahedral geometry. Shifting the junction within the dumbbell monomers either +1 or -1bp relative to the ideal location can significantly impact the geometry of neighboring rings, as indicated by the three-dimensional models.

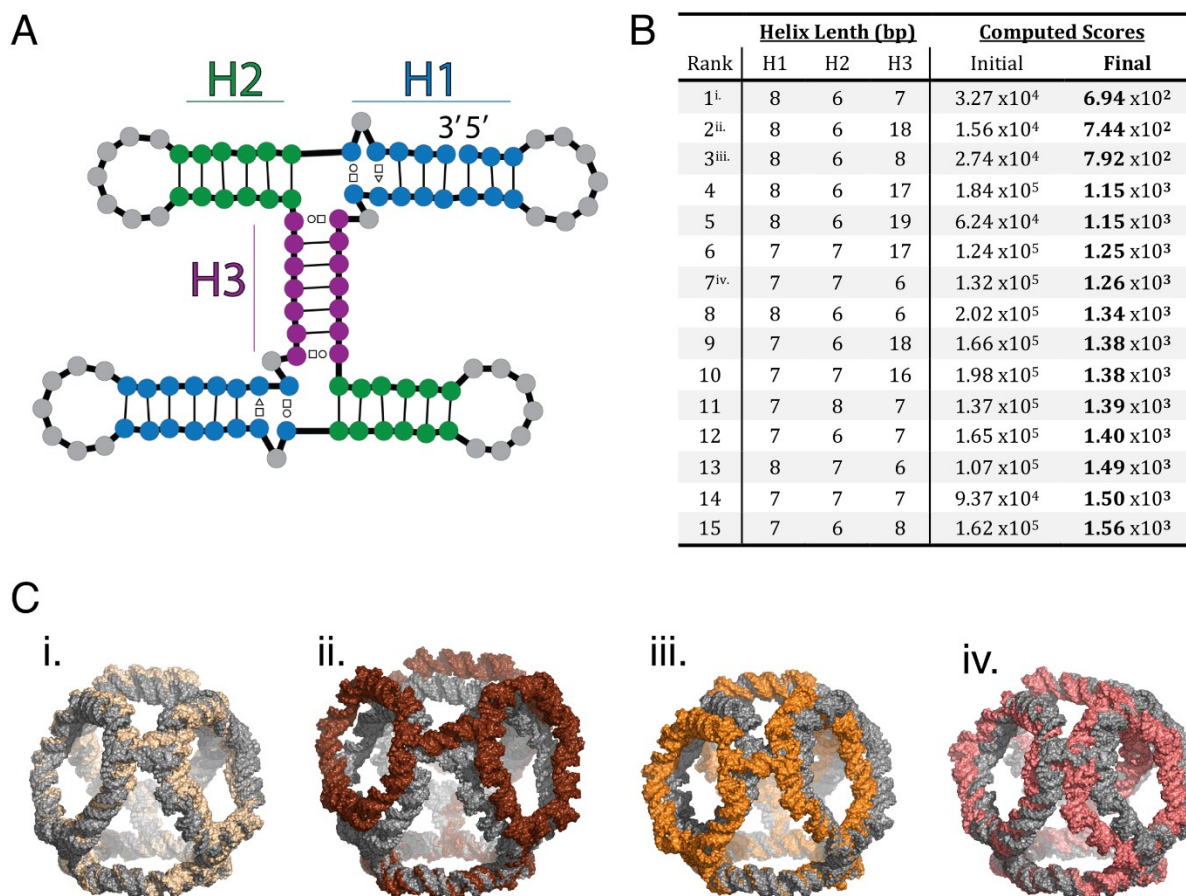


Figure S2. The ribocomb algorithm was used to verify the optimal helix lengths and junction placements within the truncated tetrahedral scaffold’s cross-over monomers. (A) Helices H1 (blue) and H2 (green) were varied in length to find the optimal placement of UAh-3WJs within the dumbbell elements. Note that helices defined as H1 and H2 exist in both dumbbell elements of the monomer. Helix H3 (purple) was varied to find the optimal distance between dumbbell elements. (B) Structures generated by ribocomb were ranked based on a computed score associated with structural strain. “Initial” scores are based on initial estimated strain of the overall tetrahedral scaffold using idealized helices. Final scores are computed after spatial optimization of motif building blocks to minimize strain of all helices. Lower scores indicate better structures. The structures of the best 15 ranked “Final” scores are listed. Superscripts in the “Rank” column correspond to structures illustrated in (C). (C) Several ribocomb-generated structures (colored) are fit to and overlaid with the manually constructed 3D model (grey) to qualitatively illustrate structural deformations due to changes in helical lengths. The initially constructed model used (H1, H2, H3) helical lengths of (8, 6, 7). The overlaid structures correspond to scaffolds with the following (H1, H2, H3) helical lengths: i. (8, 6, 7); ii. (8, 6, 18); iii. (8, 6, 8); iv. (7, 7, 6).



Figure S3. As there are six “H”-shaped cross-over monomers distributed within four rings, various distributions of the 5'/3' breaks within these cross-over monomers are possible. (A) Examples of possible distributions of cross-over monomer associated 5'/3' strand breaks. (B) A three-dimensional model subjected to molecular dynamics simulation contained a different number of cross-over monomer 5'/3' strand breaks in each of the four faces, as illustrated in the corresponding secondary structure projection. The distortion of each face relative to the initial structure was monitored throughout the simulation and reported as root mean squared deviation (RMSD).

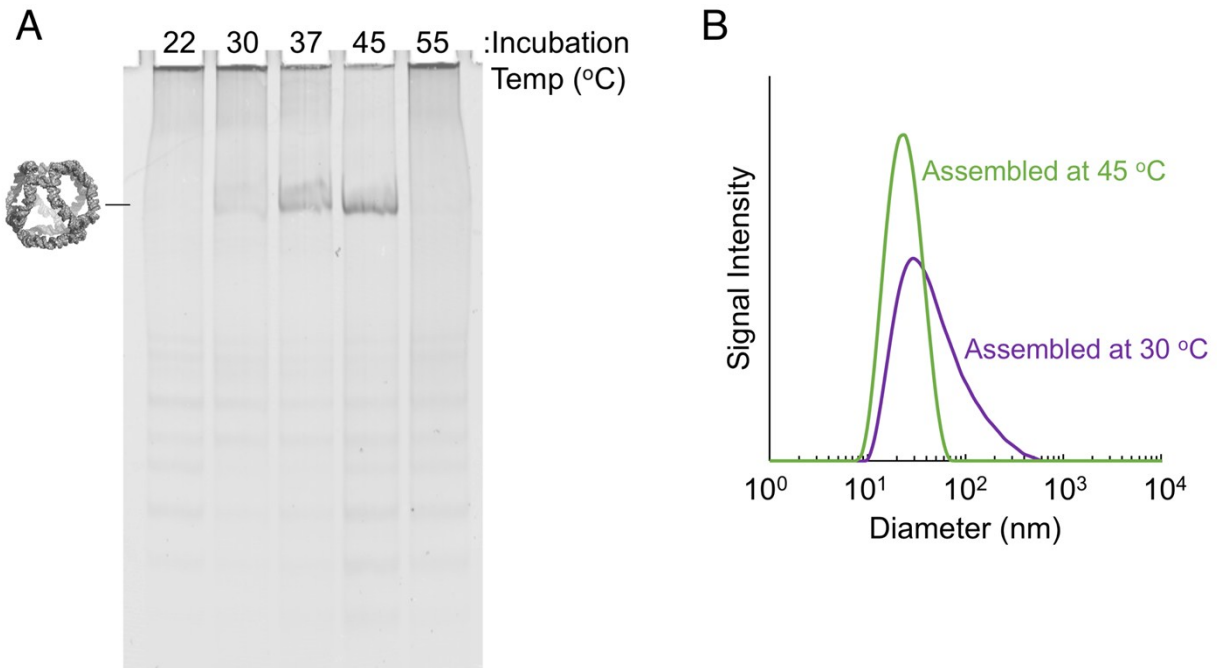


Figure S4. Various incubation temperatures were explored to promote tetrahedral nanostructure assembly. Monomer strands were mixed in stoichiometric quantities, heated to denature, snap cooled on ice, and then incubated at one of a number of different temperatures. (A) The extent of proper scaffold assembly was assessed by non-denaturing PAGE for multiple incubation temperatures. (B) Dynamic light scattering of freshly assembled tetrahedral scaffolds further indicates that using a lower incubation temperature during assembly (30 °C as compared to 45 °C) reduces the homogeneity of the resulting nanostructure and skews toward larger particle sizes.



Figure S5. Gel purified tetrahedral nanoparticles were eluted in 1x assembly buffer and continuously stored in ice. Purified nanoparticles were periodically examined by native PAGE to assess the integrity of assembled structures. Tetrahedral nanoparticles functionalized with 12 anti-eGFP DsiRNAs are shown here 17 days and 53 days post-purification, with no indications of disassembly.

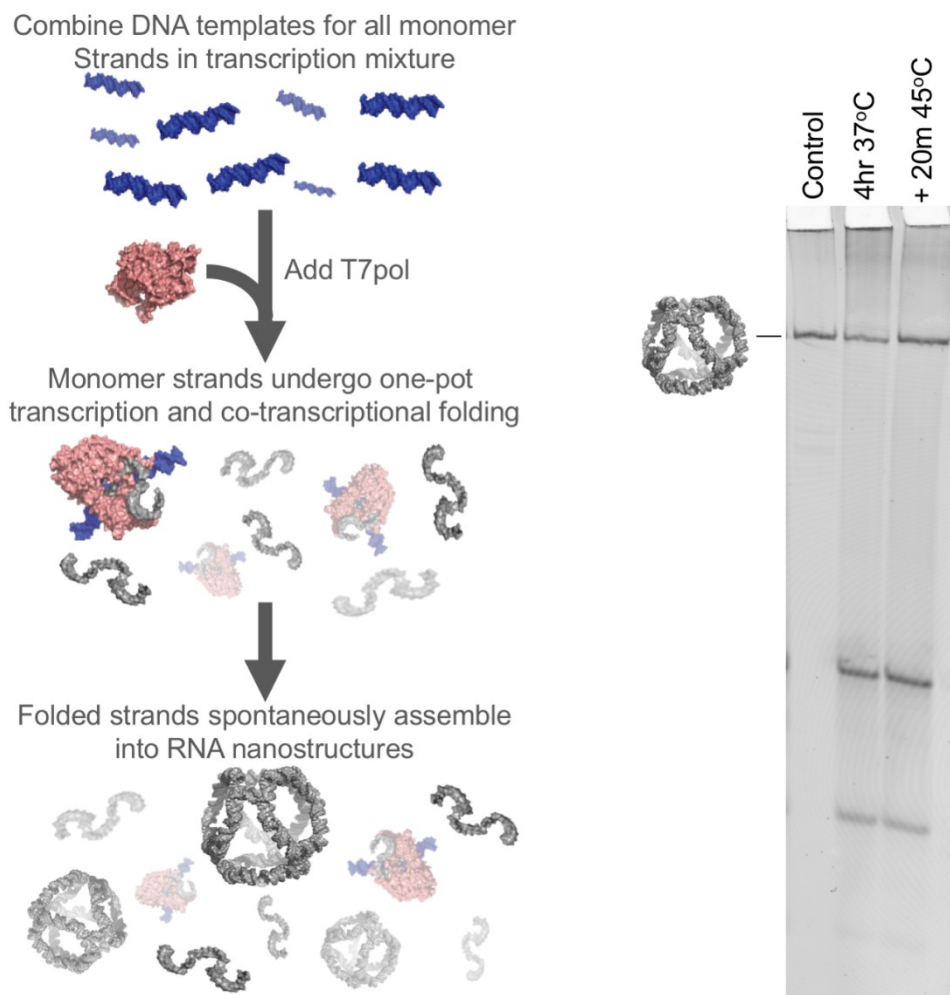


Figure S6. The tetrahedral RNA scaffold is able to assemble co-transcriptionally from the simultaneous transcription of 6 DNA templates, each encoding one monomer sequence. Co-transcription of the six templates was carried out for 4 hours at 37 °C, after which DNase was added to degrade the DNA templates. An aliquot of the sample was then removed and subjected to an additional 20 minute incubation at 45 °C, post-transcription. Nanostructure assembly was evaluated by loading a portion of the transcription mixture on a non-denaturing PAGE gel. A sample assembled from purified strands using one-pot thermal denaturation/renaturation folding was used as a properly assembled control for PAGE analysis. RNA staining was performed using ethidium bromide.

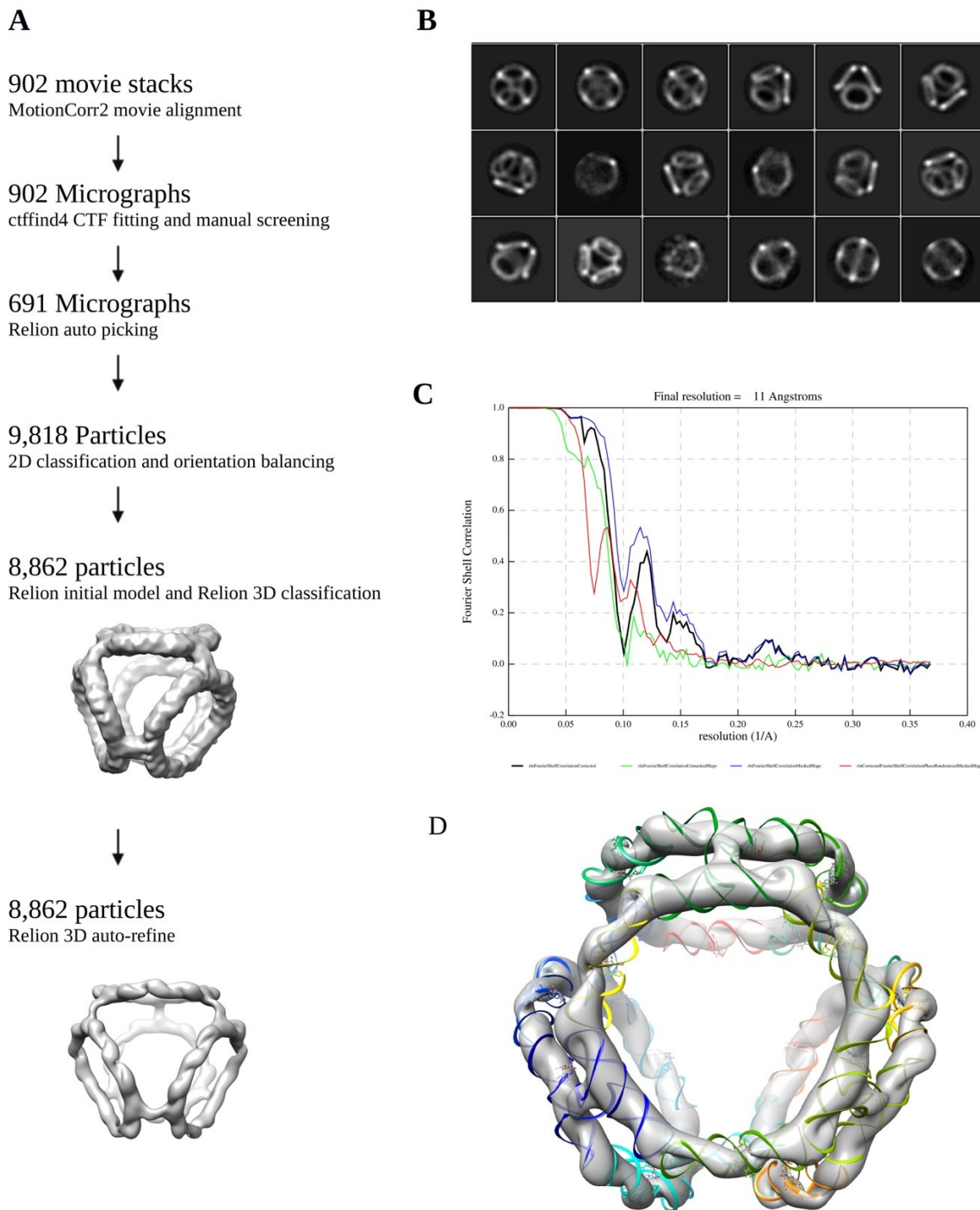


Figure S7. Cryo-electron microscopy image processing and model fitting. (A) Workflow detailing the major steps of the image processing. (B) 2D classes of the tetrahedral RNA scaffold. (C) Fourier shell correlation (FSC) curves to illustrate the final resolution at 11 Å. (D) The initial minimized computational model of the tetrahedral scaffold (used for molecular dynamics simulation portrayed in Figure 2 and Figure S3) fit to the experimentally obtained density.

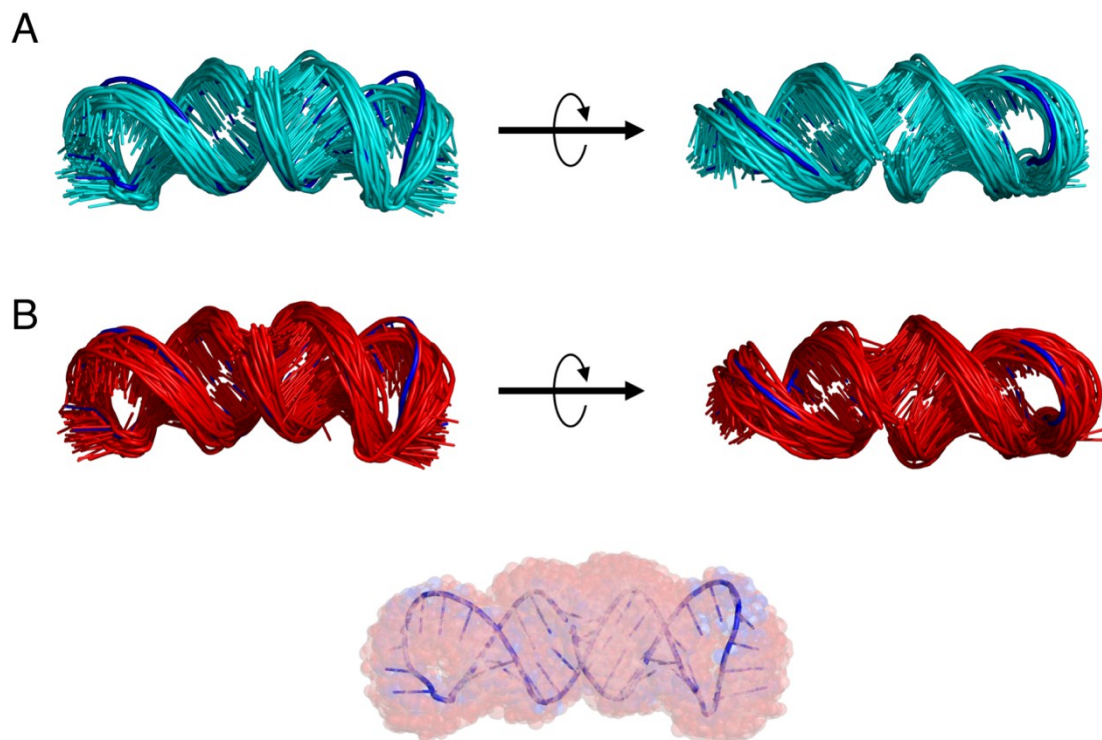


Figure S8. Observed motions within dumbbell monomers at the 5'/3' nick. Structural snapshots taken from the 250 ns molecular dynamics trajectory of the entire tetrahedral core scaffold were overlaid for two distinct monomers (A and B), each from a different face of the structure. The monomers appear to exhibit both slight opening/breathing of the 5' end and slight bending of the helical stacks at the junction at the 5'/3' junction, relative to the initial model structure (dark blue backbone). The spherical atom representation in (B) emphasizes the bending phenomena relative to the initial structure (dark blue backbone).

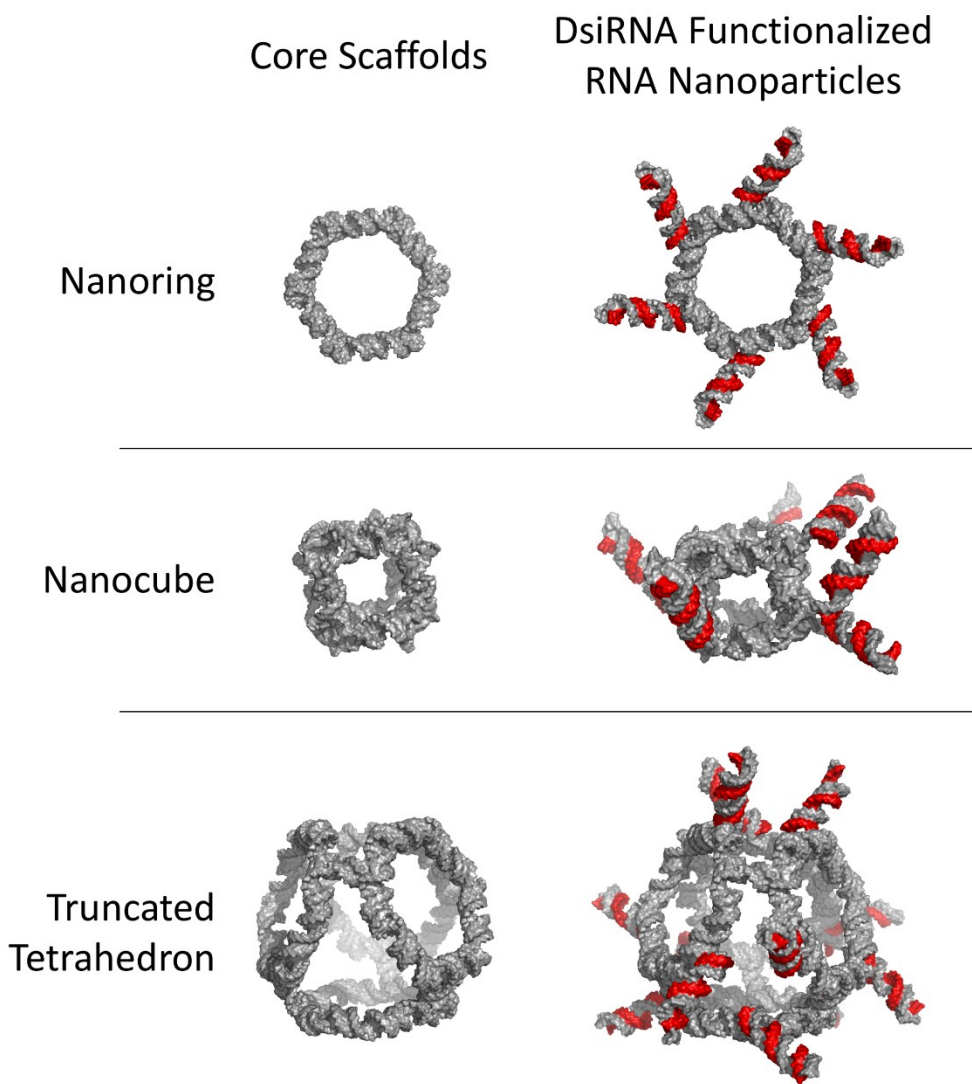


Figure S9. Three-dimensional models of the RNA nanoring (top), nanocube (middle) and truncated tetrahedron (bottom) depicting the core scaffolds (left) and DsiRNA functional nanoparticles (right) are provided. The nanoring and nanocube core scaffolds are each assembled from six distinct RNA strands. Each functionalized NP is generated in the same manner as the functionalized tetrahedral scaffold, where the 3' end of the scaffold strand is extended and encodes an antisense sequence, to which the complementary sense-coding strand is annealed. In the case of the truncated tetrahedron, only the dumbbell monomers (and not the cross-over monomers) have 3' end extensions for DsiRNA functionalization.

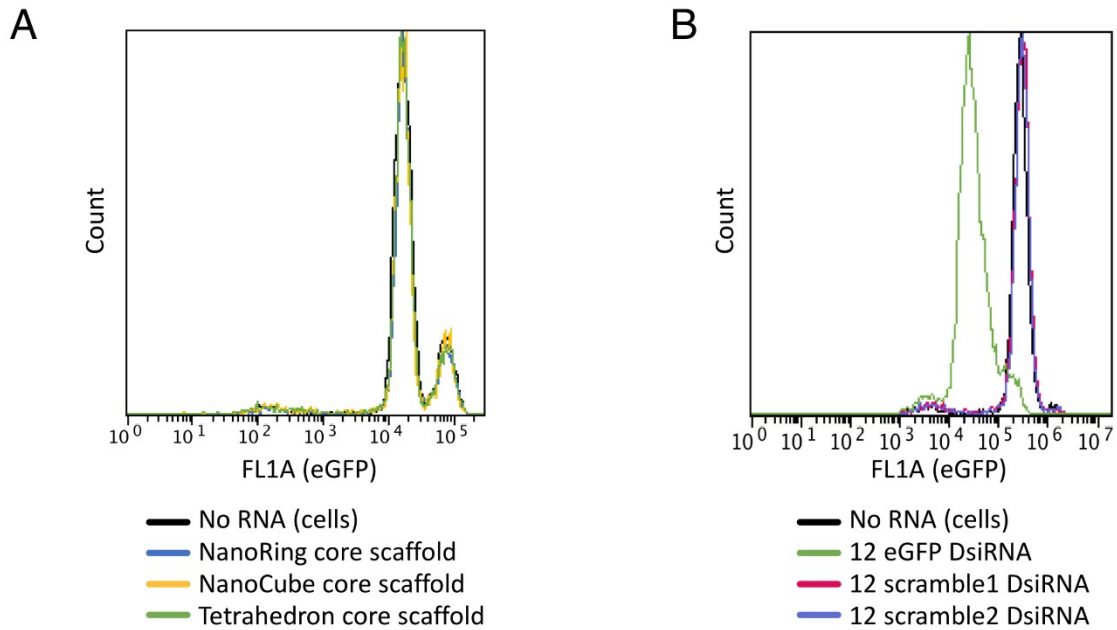


Figure S10. Several negative control transfection experiments were performed and analyzed for changes in eGFP expression. (A) “Naked” RNA core scaffolds that lack any DsiRNA appendages do not silence the expression of eGFP. The eGFP fluorescence of cells transfected with the non-functionalized nanoring, nanocube or tetrahedral core scaffolds was compared to untreated cells (black) by flow cytometry analysis three days post-transfection. (B) Tetrahedral NPs that harbor scrambled DsiRNA sequences do not down regulate eGFP expression. Two different scrambled DsiRNA sequences were incorporated into respective tetrahedral NPs and transfected into cells. eGFP fluorescence was measured three days post transfection by flow cytometry and compared to untreated cells (black), and cell transfected with eGFP targeting tetrahedral NPs.

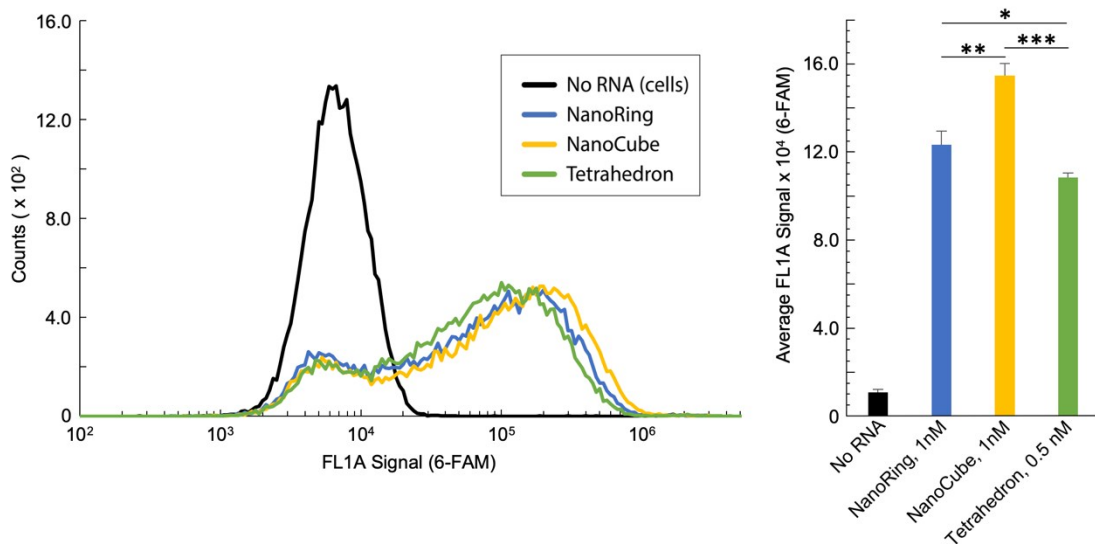


Figure S11. Cellular uptake of fluorescently labeled nanoparticles. RNA nanoparticles were assembled with their full complement of DsiRNA moieties (6 DsiRNAs for nanoring and nanocube NPs; 12 DsiRNAs for tetrahedral NPs), with four 6-FAM fluorescent labels per assembled nanoparticle. These labeled RNA NPs were transfected into MDA-MB-231 cells at normalized concentrations such that the number of DsiRNAs was equal in each transfection experiment. The extent of RNA NP uptake was assessed after four hours by flow cytometry (left). The average signal of 6-FAM fluorescence of cells treated with RNA NPs is reported following transfection at the indicated NP concentration (right). Error bars represent SD. P-values calculated by two-tailed student's t-test are indicated as follows: * < 0.05, ** < 0.01, *** < 0.001.

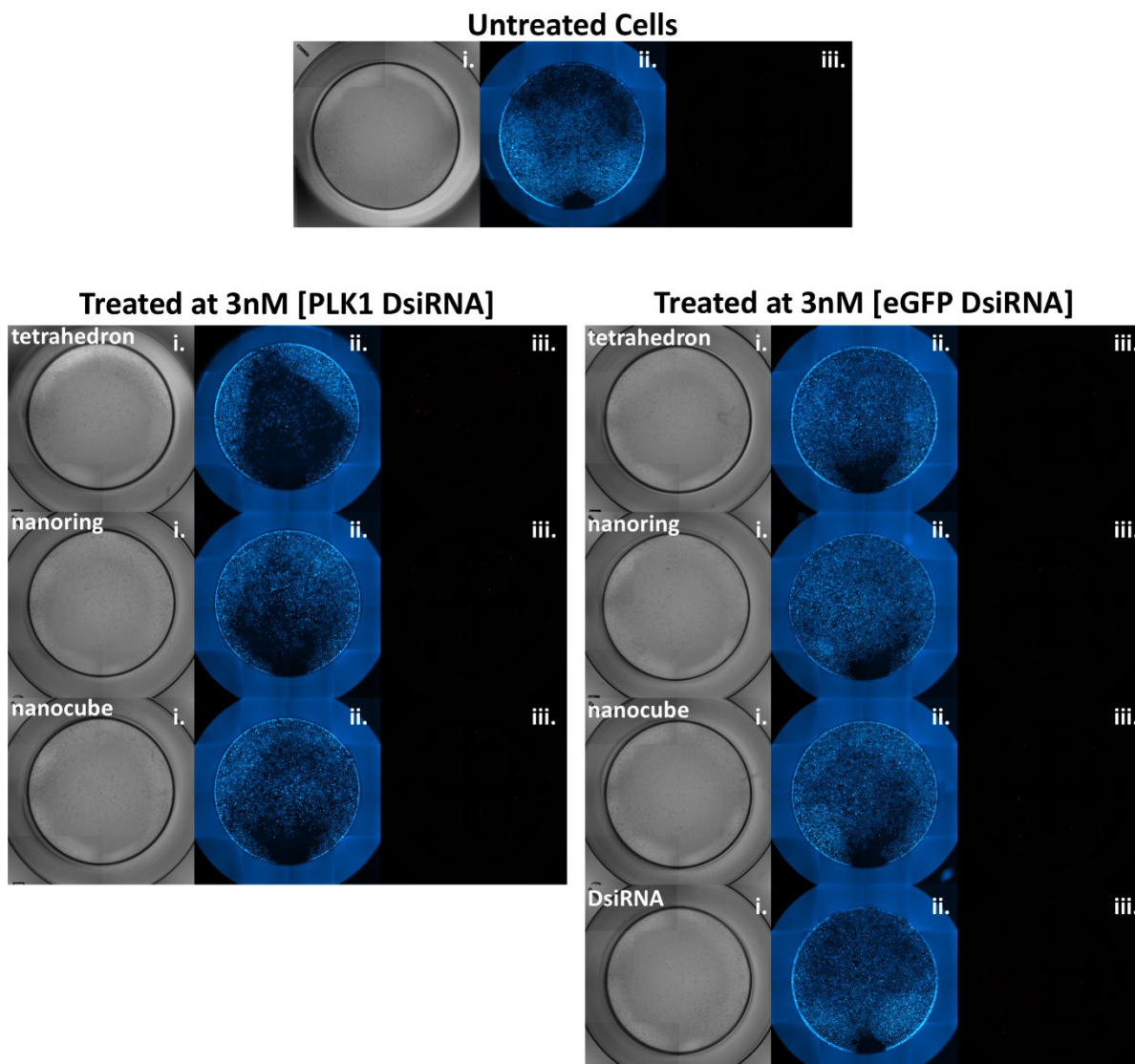


Figure S12. Relative cell viability was determined using image cytometry three days post-transfection of targeting (PLK1) and negative control (eGFP) functionalized RNA NPs. The RNA NP concentrations used for transfection were normalized based on the number of DsiRNAs harbored by each NP, such that an equimolar concentration of DsiRNA was compared between each RNA NP. Images presented are representative images from one experiment on a single 96-well plate. The representative images shown are after treatment with RNA NPs at a relative DsiRNA concentration of 3 nM, however, experiments were performed across a range of concentrations (see Figure 5 of the main text). Each well was imaged (i.) in brightfield, (ii.) for Hoechst fluorescence (total cell staining, blue) and (iii.) for propidium iodide fluorescence (dead cell staining, red). Note that minimal cells show propidium iodide fluorescence, likely due to the majority of dead cells 3 days post-transfection being removed during washing steps before and after staining. Each transfection sample was performed in triplicate wells per plate, and experimental plates were repeated three times. Relative cell viability was determined as the fraction of live cells (total cells minus dead cells) in reference to untreated control wells and reported as an average viability in Figure 5 of the main text.